# Intense rainfalls trigger nitrite leaching in agricultural soils depleted in organic matter

**Article** *in* Science of The Total Environment · February 2019

DOI: 10.1016/j.scitotenv.2019.01.306

CITATIONS
6

READS
153

**5 authors**, including:

Micòl Mastrocicco
Università degli Studi della Campania "Luigi Vanvitelli
**226** PUBLICATIONS **1,881** CITATIONS
SEE PROFILE

Nicolò Colombani
Università Politecnica delle Marche
**215** PUBLICATIONS **1,909** CITATIONS
SEE PROFILE

Elisa Soana
University of Ferrara
**48** PUBLICATIONS **745** CITATIONS
SEE PROFILE

Giuseppe Castaldelli
University of Ferrara
**163** PUBLICATIONS **2,353** CITATIONS
SEE PROFILE

# Intense rainfalls trigger nitrite leaching in agricultural soils depleted in organic matter

Micòl Mastrocicco[1], Nicolò Colombani[2#], Elisa Soana[3], Fabio Vincenzi[3], Giuseppe Castaldelli[3]

[1]DiSTABiF - Department of Environmental, Biological and Pharmaceutical Sciences and Technologies, Campania University "Luigi Vanvitelli", Via Vivaldi 43, 81100 Caserta, Italy

[2]SIMAU - Department of Materials, Environmental Sciences and Urban Planning, Polytechnic University of Marche, Via Brecce Bianche 12, 60131 Ancona, Italy

[3]SVeB - Department of Life Sciences and Biotechnology, University of Ferrara, Via L. Borsari 46, 44121 Ferrara, Italy

[#]Corresponding author: Dr, Nicolò Colombani; e-mail: n.colombani@staff.univpm.it

**Abstract**

Nitrate and ammonium are common inorganic contaminants of anthropogenic origin in many shallow aquifers around the world, while nitrite is less common, but it is most harmful than nitrate and ammonium due to its high reactivity. This paper presents evidence of nitrite accumulation after intense rainfalls in soil samples collected in an agricultural field characterized by organic matter chronic depletion. Moreover, an intact core from the same site was also collected to perform an unsaturated column experiment (60 cm long and 20 cm outer diameter) mimicking heavy rainfalls (230 mm in 2 days). Results from the field site showed nitrite accumulation (up to 0.45 mmol/kg) at 50-70 cm depth, just below the plough layer. The column experiment showed very high initial concentrations of nitrate and nitrite in the leachate and a progressive decrease of nitrate due to denitrification. The numerical flow model was calibrated versus the observed volumetric water

contents and leachate flow rates. The numerical reactive transport model was calibrated versus the leachate concentrations of six dissolved species (ammonium, nitrate, nitrite, dissolved organic carbon, chloride and bromide). The optimized model resulted to be robustly calibrated providing insights on the kinetic rates driving the production, accumulation and leakage of nitrite, showing that incomplete denitrification is the source of nitrite. As far as the authors are aware, this is the first study reporting a clear link between high nitrite leaching rates and extreme rainfall events in lowland agricultural soils depleted in organic matter. The proposed methodology could be applied to quantify nitrite cycling processes in many other agricultural areas of the world affected by extreme rainfall events.

**Keywords:** recharge; fertilizer leaching; soluble salts; agricultural soils; numerical modelling.

## 1. INTRODUCTION

Fertilizers are the major source of nitrate ($NO_3^-$) and ammonium ($NH_4^+$) contamination in both soils and groundwater in agricultural landscapes (Erisman et al. 2008; Tilman et al. 2001), and for this reason they are the most studied inorganic contaminants around the world (Nkoa 2014; Rivett et al. 2008; van Grinsven et al. 2015). In comparison, much less attention has been paid to nitrite ($NO_2^-$), since usually its concentrations are found to be by far lower than the first two inorganic nitrogen (N) species (Riley et al. 2001; Van Cleemput and Samater 1995). $NO_2^-$ is an intermediate product of many bacterial processes such as nitrification, i.e. the oxidation of $NH_4^+$ to $NO_3^-$, denitrification, i.e. the heterotrophic stepwise conversion of $NO_3^-$ to dinitrogen gas, and the dissimilatory $NO_3^-$ reduction to $NH_4^+$ (Philips et al. 2002; Rivett et al. 2008). Recent studies have highlighted that elevated $NO_2^-$ concentrations can be found in soils and porewaters if some environmental conditions occur (Castaldelli et al. 2019; Su et al. 2011), like alkaline conditions (Castaldelli et al. 2019; Shen et al. 2003), soil's water saturation state (Gelfand and Yakir 2008), presence of nitrification inhibitors (Giguere et al. 2017; Venterea et al. 2015) and lack of readily available organic substrates (Castaldelli

et al. 2013a; Kramer et al. 2006). These conditions might concur to partially inhibit nitrification and denitrification processes, thus allowing the accumulation of $NO_2^-$ in the subsurface. To date, the best practices in use in vulnerable zones aim to prevent $NO_3^-$ to exceed threshold limits in both surface (Haas et al. 2017) and groundwater (Di and Cameron 2002), but $NO_2^-$ has a much lower threshold limit (1 mg/l). Besides, $NO_2^-$ accumulation in soils can trigger greenhouse gasses production, like $N_2O$ (Giguere et al. 2017; Maharjan and Venterea 2013) and nitrous acid (Su et al. 2011). Thus, it is important to understand the mechanisms that could lead to $NO_2^-$ accumulation, transformation and leaching from agricultural soils.

Laboratory experiments (Lim et al. 2018; Tierling and Kuhlmann 2018) and particularly those performed on undisturbed soil columns under controlled conditions are an invaluable tool to grasp the main biogeochemical processes occurring in the field, such as $NO_2^-$ production and leaching in agricultural soils (Jiao et al. 2004). While the best way to quantify flow and transport dynamics in undisturbed soil column experiments is to use physically based models, which have been developed to analyse the impact of preferential water flow and physical non-equilibrium solute transport effects on soil and water resources (Köhne et al. 2009); one of the best methods for estimating parameters of the physical non-equilibrium is parameters fitting via inverse modelling under optimized experimental conditions (Colombani et al. 2014; Lee et al. 2002). Nevertheless, field data are needed to unravel the combined effects of crops rotation and climate variability. For example, the absence of cover crops combined with the increase, in the last decade, of extreme precipitation events after prolonged dry periods, have changed and will continue to change the leaching of nutrients from agricultural soils (Borken and Matzner 2009). In fact, evapotranspiration processes often lead to inorganic salts accumulation in the vadose zone during the dry season (Colombani et al. 2016; Costa et al. 2002). Besides, evapoconcentration processes accumulate inorganic pollutants, while labile organic substrates are usually oxidized (Maggi and Daly 2013), leading to C:N stoichiometrically imbalances in the unsaturated zone (Taylor and Townsend 2010). When extreme rainfall events take place, pulses of soluble salt such as $NO_3^-$ salts accumulated in the unsaturated zone over the dry

77 season might be leached down, while denitrification might be limited or stopped by the lack of labile
78 organic substrates (Castaldelli et al. 2019). For the above-mentioned reasons, $NO_2^-$ could become a
79 water pollutant of concern in the next years and not only a catalyst for atmospheric pollution (Su et
80 al. 2010) or greenhouse gasses release (Ma et al. 2015; Tierling and Kuhlmann 2018).
81 A series of soil samples were collected in the field to monitor inorganic N species evolution after
82 extreme rainfall events and an intact core column experiment was performed in the laboratory
83 mimicking the environmental conditions to quantify the processes affecting $NO_2^-$ processing and
84 leaching from agricultural soils. The column experiment outcomes were modelled with the variable
85 saturated-unsaturated flow and transport model HYDRUS-1D (Šimůnek et al. 2009) accounting for
86 chain reactions of N species, organic carbon degradation and tracers, like chloride and bromide. As
87 far as the authors are aware, this is the first study reporting a clear link between high rates of $NO_2^-$
88 leaching and extreme rainfall events in lowland agricultural landscapes.
89
90 **2. MATERIALS AND METHODS**
91
92 **2.1. Soil collection and analysis**
93
94 An assessment of mineral N species ($NH_4^+$, $NO_3^-$ and $NO_2^-$) presence in soils was performed in an
95 agricultural site (44°47’41’’N and 11°42’20’’E), located in the Po River Plain near the city of Ferrara
96 (Northern Italy). These soils pertain to freshwater paleo-river environments (Hypocalcic Haplic
97 Calcisols) and are cultivated with a rotation of wheat and maize with a N fertilization based on NPK
98 mineral fertilizers, $NH_4NO_3$ and synthetic urea with a total average rate of 170 kg N $ha^{-1}$ $y^{-1}$, since
99 this area has been declared vulnerable to $NO_3^-$ following the European Water Framework Directive
100 (2000/60/CE). A series of 5 soil samples (1 cm diameter and 20 cm long cores) were collected using
101 a hand driven auger corer. Core samples were taken randomly in the field 10 m from each other at

depth of 0-20, 50-70 and 90-110 cm below ground level (b.g.l.) to assess the horizontal and vertical variance of soil's physical properties and mineral N species concentrations.

The field was cultivated with winter wheat seeded the 30$^{th}$ of October 2016. Fertilization was done as follow: a pre-seedling fertilization the 13$^{th}$ of October 2016 (40 kg N ha$^{-1}$ of $NH_4NO_3$) incorporated by mouldboard ploughing, an after-seedling fertilization the 23$^{rd}$ of February 2017 (85 kg N ha$^{-1}$ of $NH_4NO_3$) by broadcast spreading and a pre-emergence fertilization the 3$^{rd}$ of April 2017 (46 kg N ha$^{-1}$ of synthetic urea) by broadcast spreading.

Figure 1 depicts the meteorological conditions recorded during the study period, using data from a meteorological station located approximately 250 m from the field site. The reference potential evapotranspiration rate ($Et_0$) was calculated using the Penman-Monteith equation (Allen et al. 1998). The first sampling round was performed the 21$^{st}$ of January 2017 after an anomalously dry period for this climatic zone (68 mm fallen from 01/11/2016 to 21/01/2017), where usually more than 150 mm fall during winter (Antolini et al. 2016). The second sampling round was performed the 22$^{nd}$ of February 2017 after evenly distributed rain events (52 mm fallen from 01/02/2017 to 21/02/2017). The third sampling round was performed the 26$^{th}$ of July 2017 one month after the wheat harvest with bare soil, after a prolonged summer dry period (30 mm fallen from 26/06/2017 to 26/07/2017). The forth sampling round was performed the 23$^{rd}$ of March 2018 after a prolonged wet period with bare soil (127 mm fallen from 23/02/2018 to 23/03/2018, with 63 mm fallen from 12/03/2018 to 21/03/2018). The collected soil samples were stored in polyethylene (PE) bottles and immediately frozen at -18 °C until analysed. Soil samples were homogenized at room temperature and a physical characterization was performed (Table 1).

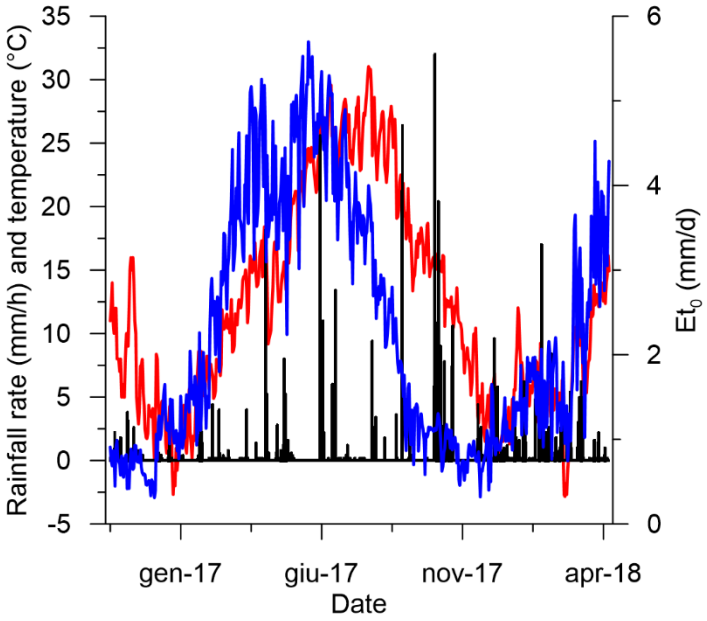


Figure 1. Rainfall events (black lines), air temperature (red line) and reference evapotranspiration (blue line) observed in a meteorological station located near the field site.

## 2.2 Column experiments

The leaching test was conducted at laboratory conditions (25±0.5 °C) using a plexiglass column with an internal diameter of 19.6 cm and a length of 60.0 cm, equipped with polyethylene post-chamber consisting of a 2.5 mm porous disc and a 2 cm layer of quartz sand, to avoid material loss. The intact soil column was collected the 18$^{th}$ of April 2018. First, the portion of soil adjacent to the column to be collected was excavated down to 60 cm, to allow the installation of 5TE Decagon probes inside the intact core at 5, 30 and 45 cm b.g.l., to monitor volumetric water content (VWC), temperature and soil bulk electrical conductivity ($EC_b$). The probes' wires were inserted into the plexiglass tube before gently pushing it through the soil profile down to 55 cm b.g.l.. While the tube was pushed down, the soil around the column was carefully removed with a shovel to allow removing the column without altering its internal structure by pushing and pulling too much. The intact core column was then transported to the laboratory and equipped at the bottom with the post-chamber.

141 The elution experiment started the 28th of May 2018 by irrigating the column with synthetic rainwater
142 using a peristaltic pump equipped with 8 tubes providing a homogeneous rainfall pattern distribution
143 on the topsoil. A total amount of 230 mm of rain was applied to the column for two days to mimic
144 the recorded rainfall pattern during an extreme rainfall event occurred in October 2017, which
145 delivered one third of the average annual precipitations usually recorded in this area (Fig. 2).
146

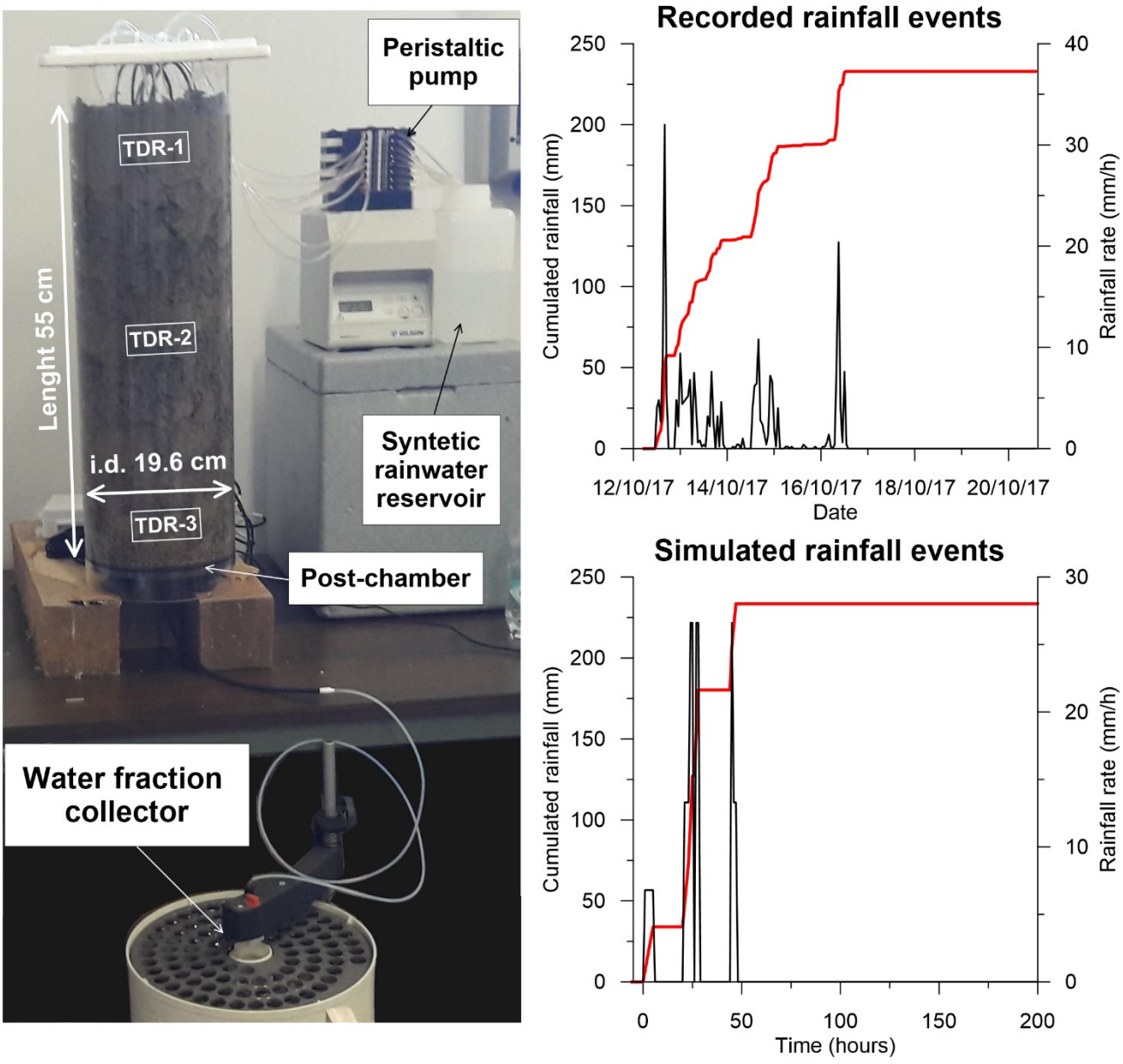


147

148 Figure 2. Scheme of the experimental setup used in the intact soil column leaching experiment (left
149 picture). Rainfall events observed in the field (upper plot) and simulated during the laboratory
150 experiment (lower plot) are represented in the right panels.

151

152 An effluent tube was fixed to a Pharmacia Lab fraction collector using 15 ml vials; collected samples
153 were divided into two aliquots for the analysis of anions, DOC and $NH_4^+$ and for pH and EC
154 measurement. Comparing the EC of the column outflow samples and their ionic strength with the
155 porewater EC derived from the $EC_b$ according to the model of Vogeler et al. (1996), a linear
156 relationship (with a slope of 0.739 and $R^2$ of 0.968) was found which allow the conversion of the EC
157 data to salinity data.
158 Sample volume was chosen to be "minimal" to avoid dilution and cross contamination between
159 successive samples. Extra column volume was considered when the experimental elution curves were
160 constructed by correcting the arrival volumes of the effluent.
161 In the first rainfall event (Fig. 1), the synthetic rainwater composition consisted of a solution of 0.1
162 mmol/l NaBr, 0.5 mmol/l $NaNO_3$ and of 0.01 mmol/l of $CaCl_2$ dissolved into double deionized water.
163 A solution of 0.01 mmol/l of $CaCl_2$ dissolved into double deionized water was injected in the other
164 rainfall events. The first rainfall event served to mimic the possible $NO_3^-$ dry and wet deposition
165 deriving from air pollution which is quite frequent in these zones (Castaldelli et al. 2013b; Ventura
166 et al. 2008). The experimental break-through curves (BTCs) were corrected by subtracting the
167 measured extra-column volumes of the tubing (10 ml) and of the post-chamber (200 ml).
168

169 **2.3 Analytical Techniques**

170

171 Core samples were split in different aliquots for mineral N species extraction, grain size distribution
172 analysis and other relevant parameters described below. Mineral N species were extracted in 2 N KCl
173 (1:10 w/v) on a rotary shaker for 1 h. $NH_4^+$ and $NO_2^-$ were analysed using a double beam Jasco V-
174 550 UV/VIS spectrophotometer, $NO_3^-$ was analysed with a Technicon Autoanalyzer II.
175 Particle size curves were obtained using mechanical sieves for the sand and the hydrometer technique
176 for the silt and clay fractions. Carbonate content in soil was determined with a Chittick gasometrical

177 apparatus. Soil and porewater pH were measured using a Hanna Instrument meter equipped with a
178 glass-body pH probe and a temperature probe for compensation. CEC data were sourced from the
179 soil online database of Emilia-Romagna region (https://agri.regione.emiliaromagna.it/Suoli).
180 Constant pressure head tests were used to infer the average saturated hydraulic conductivity ($K_s$) of
181 the column, while dry bulk density and soil moisture were determined using the gravimetric method
182 (ASTM 2010). The saturated water content ($\theta_s$) was measured at saturated condition, the residual
183 water content ($\theta_r$) was measured gravimetrically on air-dried sediments after heating for 24 hours at
184 105 °C. Soil organic matter (SOM) was measured gravimetrically on air-dried sediments after heating
185 for 24 hours at 360 °C.
186
187 Table 1. Sediment parameters and their standard deviation from quintuplicate samples.

| Parameter | 0-20 (cm b.g.l.) | 50-70 (cm b.g.l.) | 90-110 (cm b.g.l.) |
|---|---|---|---|
| Grain size (%) | | | |
| Fine Sand (0.63-2 mm) | 10.1±1.8 | 8.1±0.8 | 9.0±1.3 |
| Silt (2-63 μm) | 55.8±2.5 | 56.9±3.5 | 47.5±4.1 |
| Clay (<2 μm) | 34.1±3.0 | 35.0±2.4 | 43.5±3.1 |
| Dry bulk density (kg/dm$^3$) | 1.01±0.05 | 1.31±0.11 | 1.57±0.20 |
| Residual water content (%) | 0.03±0.015 | 0.04±0.012 | 0.04±0.031 |
| Saturated water content (%) | 44.6±0.4 | 55.3±0.4 | 55.0±0.3 |
| Soil pH (-) | 7.7±0.1 | 7.8±0.1 | 7.9±0.1 |
| SOM (%) | 1.8±0.4 | 0.5±0.1 | 0.4±0.1 |
| Carbonates (%) | 9.1±0.6 | 11.5±0.4 | 4.0±0.3 |

188
189 Online parameters on the leaching solutions were determined with an electrode conductivity cell for
190 EC measurements (Hanna Instrument). Major ions ($Cl^-$, $NO_2^-$, $Br^-$, $NO_3^-$ and $SO_4^{2-}$) were determined
191 by a 930 Metrohm ion chromatography system equipped with an ion exchange column and

192 conductivity suppressor with a detection limit of 10 µmol/l. The $NH_4^+$ and DOC concentration in
193 water were analysed using a Pharmacia 300 UV/VIS spectrophotometer with a detection limit of 1.0
194 µmol/l. Total fatty acids (TFA) were determined on a double beam Jasco V-550 spectrophotometer
195 after esterification with ethylene glycol and subsequent reduction with Fe(III) salts, with a detection
196 limit of 100 µmol/l.
197
198 **3. MODELING APPROACH**
199
200 **3.1 Flow and transport modelling**
201
202 The finite element model HYDRUS-1D (Šimůnek et al. 2009) was selected for simulating the one-
203 dimensional movement of water in variably saturated media. The program numerically solves the
204 Richards' equation for saturated-unsaturated water flow, under the assumptions that the air phase is
205 negligible and thermal gradients can be ignored in the water flow process. The van Genuchten (1980)
206 parametric functions were initially chosen to solve the Richards' equation.
207 Since the intact soil column is affected by stagnant zones and preferential pathways, the single
208 porosity approach was considered inappropriate (Larsonn and Jarvis 1999) and the dual porosity
209 approach proposed by Durner (1994) was selected. This approach divides the porous medium into
210 two overlapping regions and for each of these regions a van Genuchten-Mualem type function (van
211 Genuchten 1980) of the soil hydraulic properties is used.
212 In addition to the standard advection-dispersion equation (ADE) for the solute movement, HYDRUS-
213 1D also implements a dual domain formulation that accounts for physical non-equilibrium processes.
214 In this formulation, the pore space is conceptually divided into two distinct domains, mobile and
215 immobile (MIM) domains. In the mobile domain, transport is assumed to be governed by advection
216 and hydrodynamic dispersion. Within the immobile domain, no advective transport is assumed to
217 occur. This approach was also initially evaluated, but then discarded since for the principle of

parsimony (minimum number of parameters which lead to an effective model calibration) should be always preferred in groundwater modelling to more complex approaches if they do not substantially improve the model calibration (Hill 2006).

### 3.2 Flow and transport boundary conditions

The numerical grid was discretized in 101 nodes of 0.55 mm each to form a regular grid 55 cm long. At the soil surface, a variable pressure head/flux boundary condition was selected to reproduce changes in infiltration rate due to different rainfall intensity. As lower boundary condition, a zero-gradient boundary was specified to simulate a freely draining soil profile, since capillary rise from the water table is negligible in this area, being the groundwater depth from surface usually more than 2 m.

In the transport model, a third-type (Cauchy) concentration flux boundary condition, with user specified liquid phase concentration of the infiltrating water, was selected as upper boundary, to simulate the synthetic rainwater concentration. A zero-concentration gradient (free drainage) was applied as lower boundary at the bottom of the column to simulate the outflow of the chemical species towards the saturated zone.

The reactive network model used to simulate the sequential transformations of the N species (from urea to $NH_4^+$, $NO_2^-$ and $NO_3^-$) was the one proposed by van Genuchten (1985), coupled with linear sorption for $NH_4^+$ and ammonia volatilization via a first order reaction (Šimůnek et al. 2009). The original model formulation (Eq. 1-3) was changed to account also for heterotrophic denitrification (Eq. 6 and 7) via DOC ($CH_2O$) oxidation. Dissolution of SOM was accounted for using a zero-order dissolution rate. While, $NO_2^-$ formation through partial denitrification into $NO_2^-$ (Eq. 6), denitrification to dinitrogen (Eq. 7) and $CH_2O$ bulk oxidation via oxygen and $NO_3^-$ were all modelled using first-order rate constants (Eq. 5, 6 and 7).

$$(NH_2)_2CO + H_2O \rightarrow CO_{2(g)} + 2NH_{3(g)} \quad (1)$$

$$NH_{3(g)} + H_2O \rightarrow NH_4^+ + OH^- \quad (2)$$

$$NH_4^+ + 2O_2 \rightarrow NO_2^- + 2H_2O \quad (3)$$

$$NO_2^- + 0.5O_2 \rightarrow NO_3^- \quad (4)$$

$$CH_2O + 0.5O_2 \rightarrow HCO_3^- + 0.5H_2O \quad (5)$$

$$CH_2O + 2.33NO_3^- \rightarrow HCO_3^- + 0.33H^+ + 2.33NO_2^- + 0.33H_2O \quad (6)$$

$$CH_2O + 1.2NO_2^- \rightarrow HCO_3^- + 0.2H^+ + 0.6N_2 + 0.4H_2O \quad (7)$$

The initial species concentrations were linearly interpolated throughout the model profile using the observed concentrations collected and analysed in the 3 soil horizons in which the column was subdivided (See supplementary information).

The linear sorption coefficients were estimated using CEC of each soil (Erskine 2000), while first order volatilization rates were estimated from laboratory experiments on ammonia volatilisation conducted in nearby fields (Castaldelli et al. 2018). Diffusion values, like molecular diffusion in water ($1.80e^{-5}$ m/h) and in air and Henry coefficient for ammonia ($4.16e^{-3}$ m/h) were kept constant in all the horizons.

Every single species was also simulated moving through the soil as non-sorbing non-degrading species to compare the non-reactive model results with the reactive model results to derive the deviation from their theoretical conservative behaviour.

### 3.3 Model calibration

The model calibration target was to minimize the differences between observed and calculated outflow and tracer concentrations from the columns. The flow and transport parameters were assumed to be homogeneous throughout the soils columns, thus they were kept constant within each model.

The flow and transport model parameters were calibrated using the inverse modelling procedure present in HYDRUS-1D, which uses a Marquardt-Levenberg type algorithm for parameter optimization. The optimized flow parameters were $\alpha$ and $n$ of the van Genuchten (1980) parametric functions in the 3 horizons constituting the intact soil column, for a total of 6 parameters which became 12 optimized parameters for both the two overlapping regions of the Durner (1994) approach. The optimized transport parameters were: vertical dispersivity $\lambda_v$ (cm), partial denitrification rate (1/d), denitrification rate (1/d), SOM dissolution rate (1/d) and $CH_2O$ oxidation rate (1/d). All these parameters were kept constant throughout the 3 horizons constituting the intact soil column, to minimize the number of parameters to optimize following the parsimony principle cited above. Other reaction parameters listed in table 3 were sourced by a similar model previously developed for these soils (Castaldelli et al. 2018).

The degree of model calibration was assessed by calculating and comparing the modelling efficiency (EF) calculated according to Nash and Sutcliffe (1970):

$$EF = 1 - \frac{\sum_{j=1}^{n}\left(O_j - P_j\right)^2}{\sum_{j=1}^{n}\left(O_j - O\right)^2} \quad (8)$$

where $P_j$ is the calculated value corresponding to the observed $O_j$, and $O$ is the mean value of the observed data.

### 3.4 Reactive modelling for saturation indices calculation

The geochemical model PHREEQC-3 (Parkhurst and Appelo 2013) was employed to calculate the equilibrium water speciation and the saturation indices (SI) for various mineral phases such calcite, dolomite, $CO_2$ partial pressure and p*e* of the solution to evaluate the redox conditions. SI is an index indicating whether the water phase will dissolve or precipitate a mineral phase based on its thermodynamic stability. SI is negative when the mineral may dissolve, positive when it may

294 precipitate, and zero when the water and mineral phases are at thermodynamic equilibrium. The input
295 values are reported in Supplementary Information.
296
297 **4. RESULTS AND DISCUSSION**
298
299 **4.1 Field mineral N species temporal evolution**
300
301 The first sampling campaign highlighted a residual $NO_3^-$ content in the upper soil horizon of 4.5
302 mmol/kg which is typical for this agricultural landscape in winter time (Castaldelli et al. 2013b), with
303 a decreasing concentration trend towards the deep soil horizons. $NH_4^+$ and $NO_2^-$ show low
304 concentrations in the upper ploughed layer, while their concentrations increase slightly with depth;
305 although, the maximum concentrations found are below 0.5 mmol/kg (Fig. 3).
306

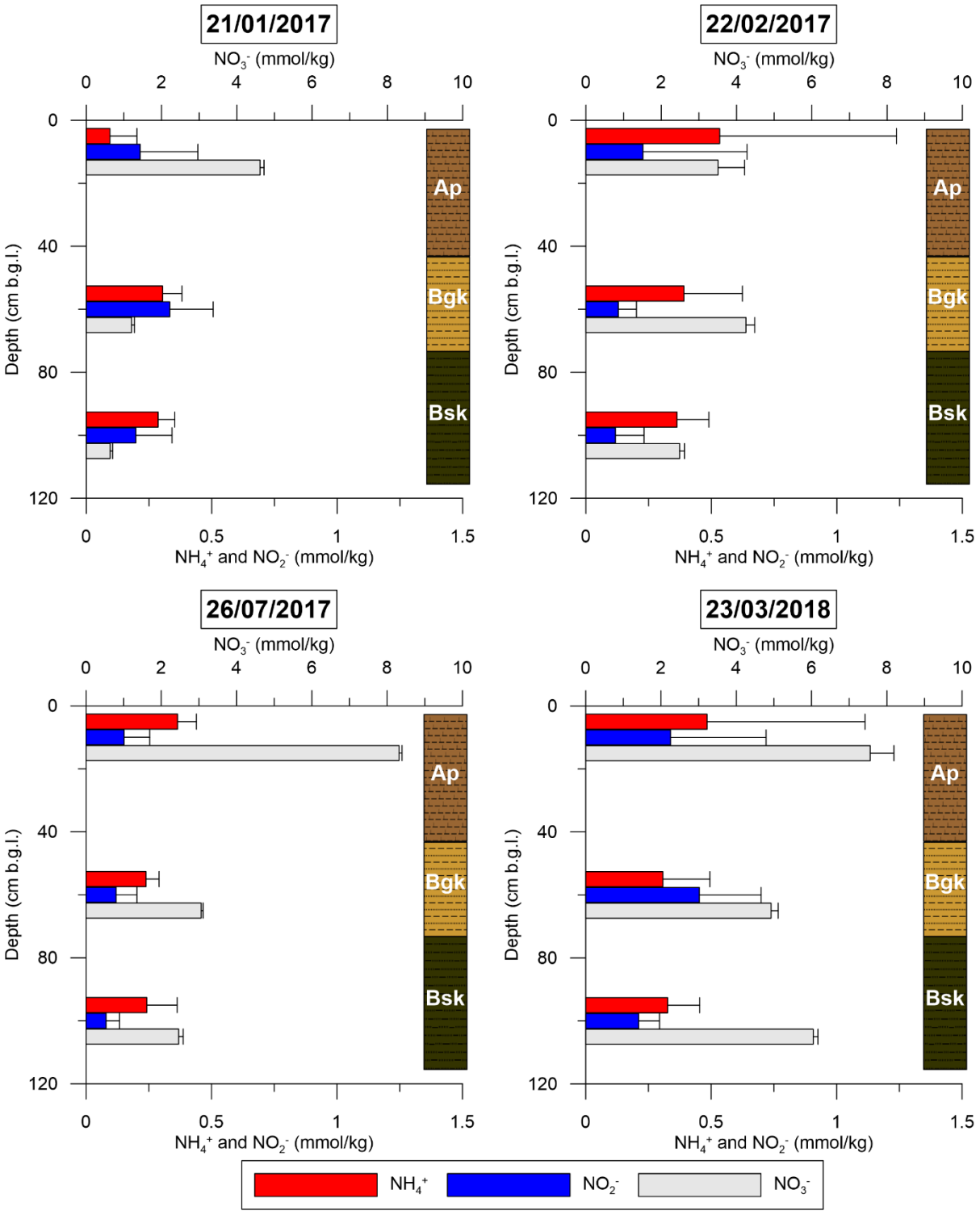


Figure 3. Depth profiles of mineral N species extracted from soils in four sampling campaigns. Error bars denote standard deviations calculated on five replicate samples.

In the second campaign, the $NH_4^+$ concentration increases in the topsoil showing a large spatial variability, denoted by the high samples' standard deviation. Since no fertilizer was applied between

313 the first and second campaign, the $NH_4^+$ increase could be due to organic N mineralization processes
314 and to the establishment of reducing conditions in micro-niches favouring DNRA (Chen et al. 2015;
315 Friedl et al. 2018). $NO_3^-$ decrease in the topsoil was most probably due to leaching towards the deeper
316 soil horizons, and only partially due to crops, fungi and bacteria assimilation processes. $NO_2^-$
317 concentrations were low along the whole soil profile since the period was characterized by evenly
318 distributed rainfall events (Fig. 1), providing optimal conditions for reactive N transformation. In the
319 third campaign $NH_4^+$ concentrations were lower than in the previous campaign in all the investigated
320 soil horizons; $NO_3^-$ concentrations were very high only in the topsoil, due to the fertilizer's leftover
321 after the harvest. Again, $NO_2^-$ concentrations were low since the period was characterized by scarce
322 rainfall, mainly summer storms events (Fig. 1) and the low soil water content inhibited microbial
323 activities. The last field campaign showed $NH_4^+$ concentrations similar to the concentrations of the
324 second campaign, while $NO_3^-$ and $NO_2^-$ concentrations were among the highest recorded in the four
325 campaigns, with relatively high concentrations also in the lower soil horizon. The increase of all the
326 mineral N species could be due to organic N mineralization, since after harvest the soil was left bare
327 and no fertilizer was applied. Besides, atmospheric deposition could have played a role, although only
328 of minor entity since the measured yearly deposition in these areas is approximately 14 kg N/ha/y
329 (Castaldelli et al. 2013b; Ventura et al. 2008).
330 Considering an average dry bulk density of 1.01±0.05 kg/dm$^3$ in the investigated topsoil of 20 cm,
331 this can be converted into 0.34±0.02 mmol/kg of reactive N deposited between the third and fourth
332 sampling campaign. The above-mentioned reactive N atmospheric load is maybe enough to explain
333 the topsoil mineral N species variations, but surely not enough to explain the $NO_3^-$ variations observed
334 in the deeper soil horizons, which passed from 3 mmol/kg in the third campaign to 5-6 mmol/kg in
335 the fourth campaign. The field monitoring highlighted the predominance of $NO_3^-$ over $NH_4^+$ and $NO_2^-$
336 as main mineral N species in the investigated soils but was unable to give insights on $NO_2^-$
337 accumulation, which was already shown in soil batch experiments using similar soils (Mastrocicco et
338 al. 2011; Mastrocicco et al. 2019).

339 Thus, even though mineral N soil extraction could be cheaper and less time consuming with respect
340 to column experiments, they do not provide solutes concentration changes over time. Therefore,
341 ultimately, column experiments are unavoidable to describe solutes fate's in soils in a realistic manner
342 (Köhne et al. 2009).
343
344 **4.2 Column experiments**
345
346 **4.2.1 Numerical flow model results**
347
348 The flow model was calibrated versus the continuous monitoring of VWC via TDR probes and the
349 observed outflow fluxes (Fig. 4). The obtained soil retention curve parameters (Tab. 2) are typical of
350 the silty clay soil constituting the intact soil column and are also realistic estimates since the statistical
351 indicator of the model fit is very good (EF = 0.911). The undisturbed soil column showed a very slow
352 outflow rate, given its low $K_s$ values (Tab. 2). For this reason, the column elution experiment took
353 more than 200 hours, with a very low total cumulative leachate amount, only 27.4 mm versus 233
354 mm of cumulative rainfall. The dual domain approach employed to simulate the flow was
355 indispensable to avoid an unrealistic water accumulation on the soil surface, which would instead be
356 formed with the single porosity approach, given the low $K_s$ values and the extremely elevated
357 precipitation rate (Larsson and Jarvis 1999); nevertheless, this complex approach can be skipped for
358 evenly distributed rainfalls, even in the low $K_s$ soils typical of this area (Colombani et al. 2014).
359 Column outflow rate was accurately reproduced by the flow model, although some uncertainties on
360 the uniqueness of the parameters cannot be excluded (Zhang et al. 2006).
361

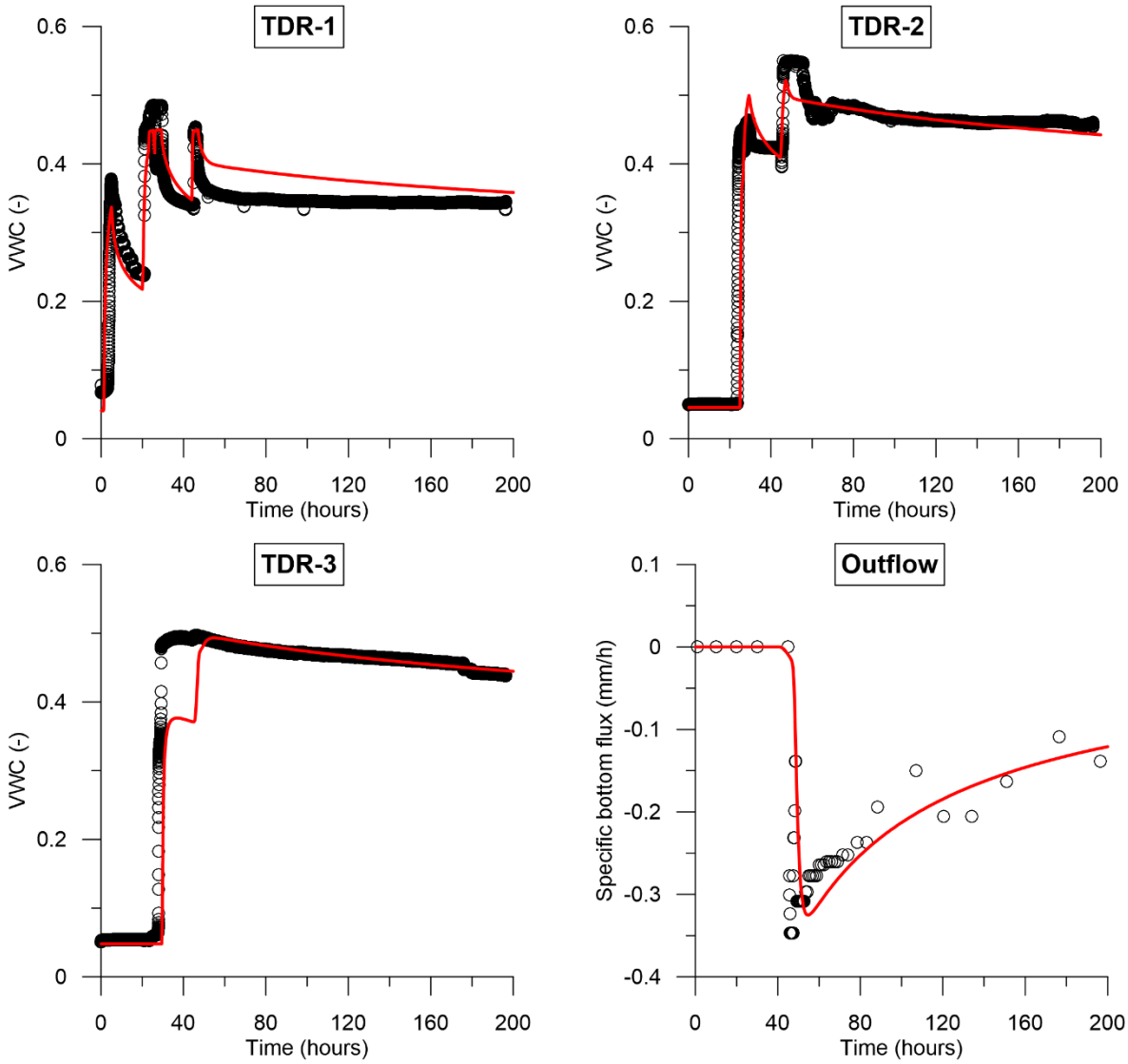


Figure 4. Comparison of observed and calculated VWC and cumulative outflow flux in the column experiment.

Table 2. Flow parameters obtained by inverse modelling for the intact soil column experiment.

| Parameter | Horizon 1 | Horizon 2 | Horizon 3 |
|---|---|---|---|
| $n$ (-) | 1.71 | 1.71 | 1.71 |
| $\alpha$ (1/m) | 0.25 | 0.25 | 0.25 |
| $K_s$ (m/d) | 0.096 | 0.094 | 0.048 |
| $n$-2 (-) | 1.5 | 1.5 | 1.5 |
| $\alpha$-2 (1/m) | 0.20 | 0.20 | 0.20 |

### 4.2.2 Soil salinity monitoring

Figure 6 shows the evolution of porewater salinity in the intact soil column exposed to extreme rainfall events. A small peak of 1.1 g/l was detected by the upper TDR probe during the first rainfall event, followed by a stabilized salinity around 0.9 g/l in the first 20 hours of the experiment. Then, the two in line rainfall events (Fig. 2) induced two negative salinity peaks due to a dilution effect, the same apply for the last rainfall event. After that, salinity stabilized to a concentration of approximately 0.84 g/l. The TDR probe located in the middle of the soil column, showed a sharp salinity jump when the water front breakthrough, with a maximum concentration of 3.6 g/l, followed by a dilution front and a slow recovery towards a stable concentration of 1.0 g/l. The lower TDR probe showed the same salinity jump with a peak of 4.6 g/l, then a dilution front and a second smoothed peak of 1.7 g/l followed by a decreasing trend towards a nearly stable concentration of approximately 1.4 g/l. The observed outflow water salinity displayed a pattern similar to the lower TDR probe, with a very high initial salinity followed by rapid fluctuations between 2.7 to 1.8 g/l and reaching a stable concentration near 2 g/l at the end of the experiment. The observed increasing salinity with depth and the sharp increase once the water front migrates downward is typical of rapidly dissolving salts that are taken into solution by the advancing water front (Colombani et al. 2014). This is frequent in desiccated soils, where soluble salts tend to precipitate in the interconnected pore space of the soil matrix (Hillel 1998).

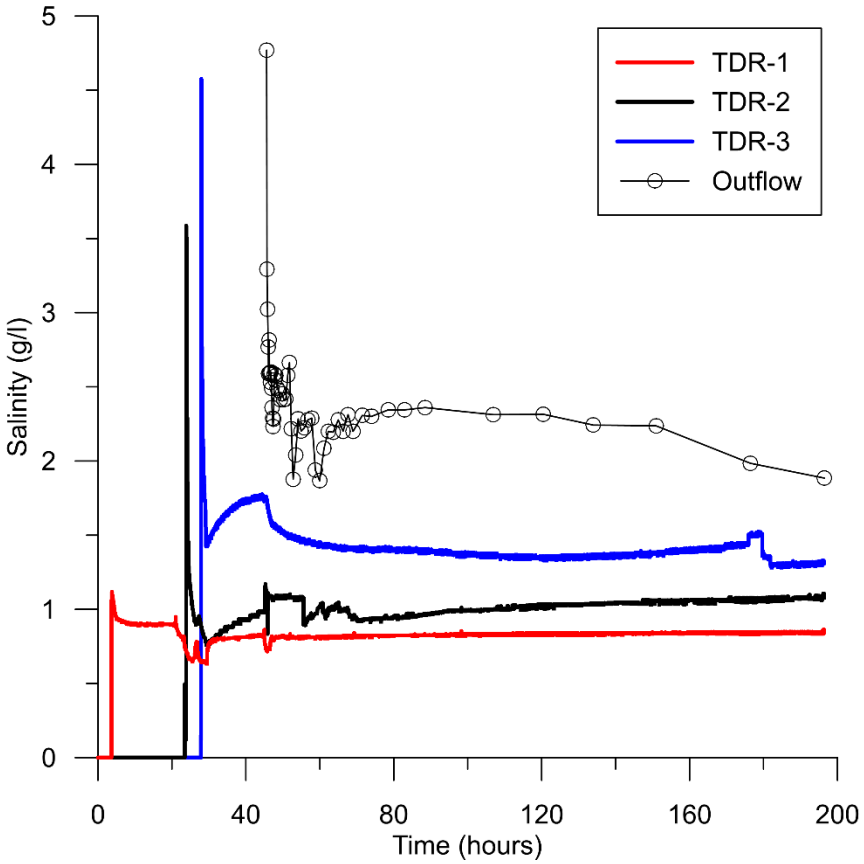


Figure 5. Continuous salinity monitoring within the soil column using TDR probes (see Fig. 2 for location) and observed salinities in the outflow samples.

### 4.2.3 Numerical reactive transport model results

The elution of both $Cl^-$ and $Br^-$ could be well fitted using the standard ADE equation (Tab. 3), since the EF (-) equal to 0.871. Thus, for the principle of parsimony, there was no need to use the more complex MIM approach. The obtained $\lambda_v$ value was relatively large, indicating a great soil heterogeneity, also confirmed by the grain size analysis (Tab. 1). Nevertheless, this value is within the range of the observed $\lambda_v$ values for undisturbed soil columns (Perfect et al. 2002), with a small 95% confidence interval indicating little uncertainty in the parameter identification.

401 Table 3. Transport parameters obtained by inverse modelling for the BTCs simulations in the intact
402 soil column. The symbol ± denotes the 95% confidence interval of the obtained parameter value.

| Parameter name | Optimized value | Equation |
|---|---|---|
| $\lambda_v$ (cm) | 2.03±0.05 | |
| *$K_d$-$NH_4^+$ ($m^3$/mol) | $4.14x10^{-7}$±$1.3x10^{-8}$ | |
| *$K_d$-DOC ($m^3$/mol) | $1.03x10^{-6}$±$1.0x10^{-7}$ | |
| *$NH_4^+$→ $NO_2^-$ (1/h) | 0.05±0.01 | Eq. 3 |
| *$NO_2^-$→ $NO_3^-$ (1/h) | 0.011±$1.9x10^{-3}$ | Eq. 4 |
| $NO_3^-$→ $NO_2^-$ (1/h) | $1.0x10^{-3}$±$3.1x10^{-4}$ | Eq. 6 |
| $NO_2^-$→ $N_2$ (1/h) | $1.93x10^{-3}$±$4.0x10^{-4}$ | Eq. 7 |
| SOM→DOC (mol/$m^3$/h) | $2.02x10^{-9}$±$3.3x10^{-10}$ | |
| $CH_2O$→ $HCO_3^-$ (1/h) | $5.11x10^{-3}$±$4x10^{-4}$ | Eq. 5, 6 and 7 |

403 ** from Castaldelli et al. (2018)*

404

405 From figure 6, the elution of conservative species like $Cl^-$ was well reproduced by the numerical
406 model, while $Br^-$ was less well reproduced especially after the first arrival, due to a dilution effect
407 followed by a rebound effect, most probably imputable to back diffusion from stagnant zones (here
408 not modelled). As previously shown in figure 6, the soluble salts were dissolved and carried by the
409 water phase at the wetting front, thus producing extremely high concentrations at the very beginning
410 of the elution phase in all the ionic and non-ionic species (Supplementary Information). $NH_4^+$ was
411 retained by the soil and showed very low concentrations in the aqueous phase, as shown by the
412 comparison between the reactive simulation and the conservative one (Fig. 7). Nevertheless, the
413 nitrification process produced a positive cumulative $NO_2^-$ mass flux of +12.1 mmol/$m^2$ (Eq. 4), while
414 the denitrification process produced a cumulative $NO_2^-$ mass flux of +25.9 mmol/$m^2$ (Eq. 5).

415

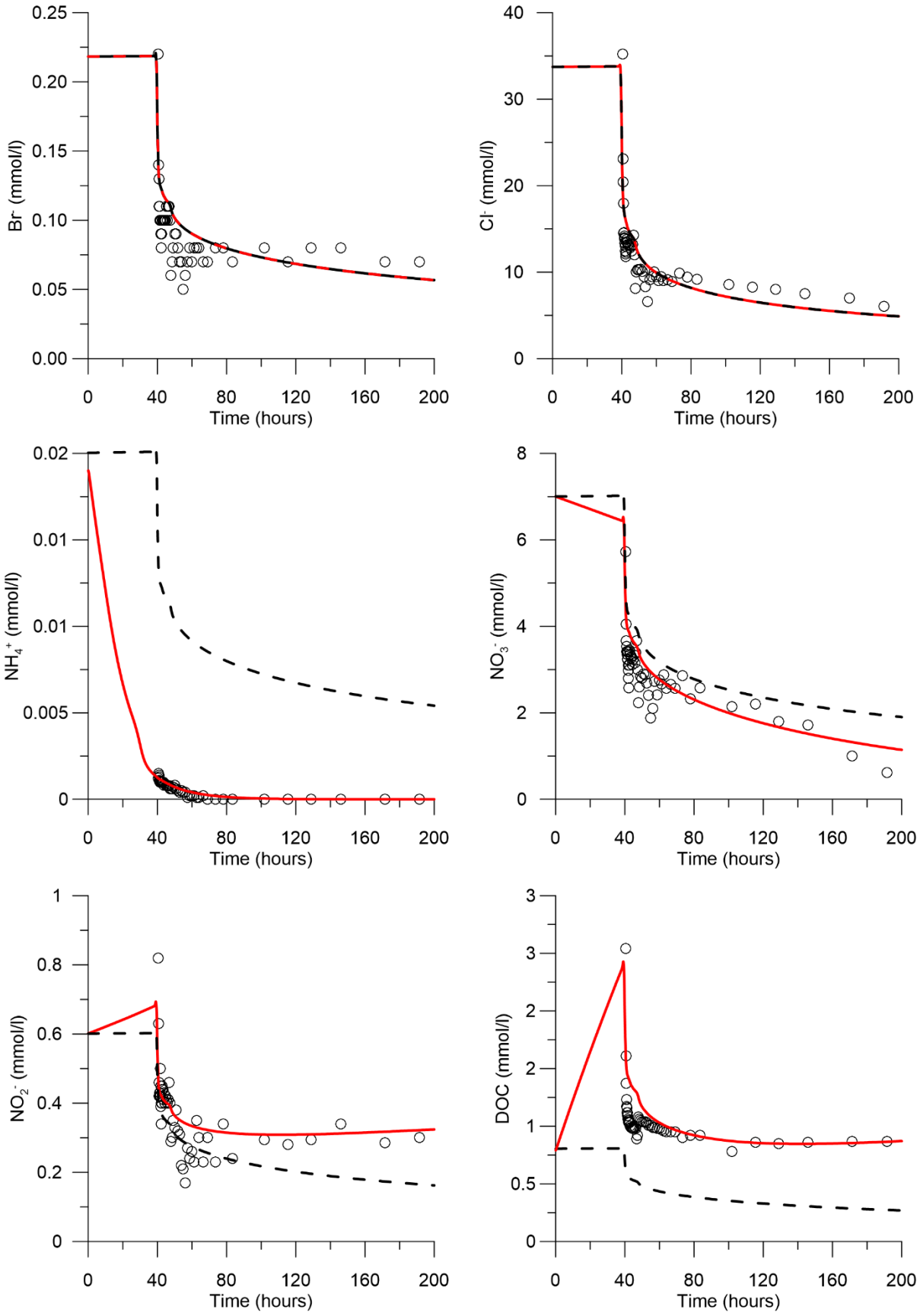


Figure 6. Observed and calculated dissolved species concentrations eluted from the intact soil column. Dashed black lines show non-reactive solute transport model results.

419 Both processes produced a transient $NO_2^-$ accumulation in the soil profile, but the prevailing process
420 was the denitrification one. In fact, for the simulated extreme rainfall event, the $NO_2^-$ mass produced
421 by denitrification was approximately twice respect to the $NO_2^-$ mass produced by nitrification.
422 The denitrification process tends to diminish $NO_2^-$ mass in the soil (Eq. 7), with a cumulative $NO_2^-$
423 mass flux of -4.42 mmol/m$^2$ (negative values indicate mass removal from the simulated domain).
424 This amount is much less than the $NO_2^-$ mass produced by partial nitrification and denitrification
425 processes (Eq. 3 and 6), explaining the slightly increasing trend of $NO_2^-$ concentrations in the outflow
426 samples with time, compared with the conservative simulation (Fig. 6). DOC was produced by
427 leaching of the more soluble SOM fraction, retained by the soil, and oxidized by both dissolved
428 oxygen in rainwater and denitrification reactions. Accordingly, since oxygen concentration in
429 equilibrium with the atmosphere at 25 °C is approximately 0.125 mmol/l, DOC oxidation rate has
430 been set higher than the mineralization rate of $NO_3^-$ and $NO_2^-$ (Eq. 6 and 7) to account for both electron
431 acceptors used by bulk DOC mineralization rate. The SOM dissolution into DOC produced a positive
432 cumulative DOC mass flux of +261.0 mmol/m$^2$ in the intact soil column. The DOC mineralization
433 produced a negative cumulative DOC mass flux of -103.8 mmol/m$^2$ (Eq. 5, 6 and 7). This amount is
434 much less than the DOC mass produced by SOM dissolution, explaining the linear increasing trend
435 of DOC concentration during the wetting stage, compared with the conservative simulation (Fig. 6).
436 The calibrated model shows an overall good performance (EF = 0.871) and a good match between
437 observed and calculated concentrations (Fig. 6). Thus, the quantified cumulative mass fluxes can be
438 considered reliable estimates of the field processes that could occur during extreme rainfall events
439 after dry periods in lowland agricultural soil depleted in organic matter.
440 Namely, a negligible $NH_4^+$ cumulative mass flux is calculated by the model, the net $NO_2^-$ mass flux
441 derived from nitrification is 2.35 mmol/m$^2$ and the one derived from denitrification is 5.65 mmol/m$^2$
442 (for a total amount of 8.0 mmol/m$^2$), the net cumulative $NO_3^-$ mass flux is 54.6 mmol/m$^2$, and the net
443 cumulative DOC mass flux is 25.0 mmol/m$^2$, with a net imbalance between electron acceptors ($NO_3^-$
444 and $NO_2^-$) and electron donors (DOC) due to fast leaching of the electron acceptors respect to the

DOC, which is retarded by adsorption processes. The presence of oxidizing conditions is also confirmed by the PHREEQC-3 calculated p*e* values, which increased rapidly from 7.0 at the beginning of the elution to 8.0, stabilized around this value, and descended towards 7.5 at the end of the experiment (Fig. 7). In addition, the fraction of TFA is very low compared with DOC (Supplementary Information), further limiting the denitrification capacity of these soils during extreme rainfall events (Oh and Silverstein 1999). On the other hand, the pH range was limited by the carbonates buffering effect (6.7<pH>7.3), thus not affecting the nitrification and denitrification rates. As a proof of this, calcite displays an initial oversaturation and a gradual tendency to under-saturation values (Fig. 8).

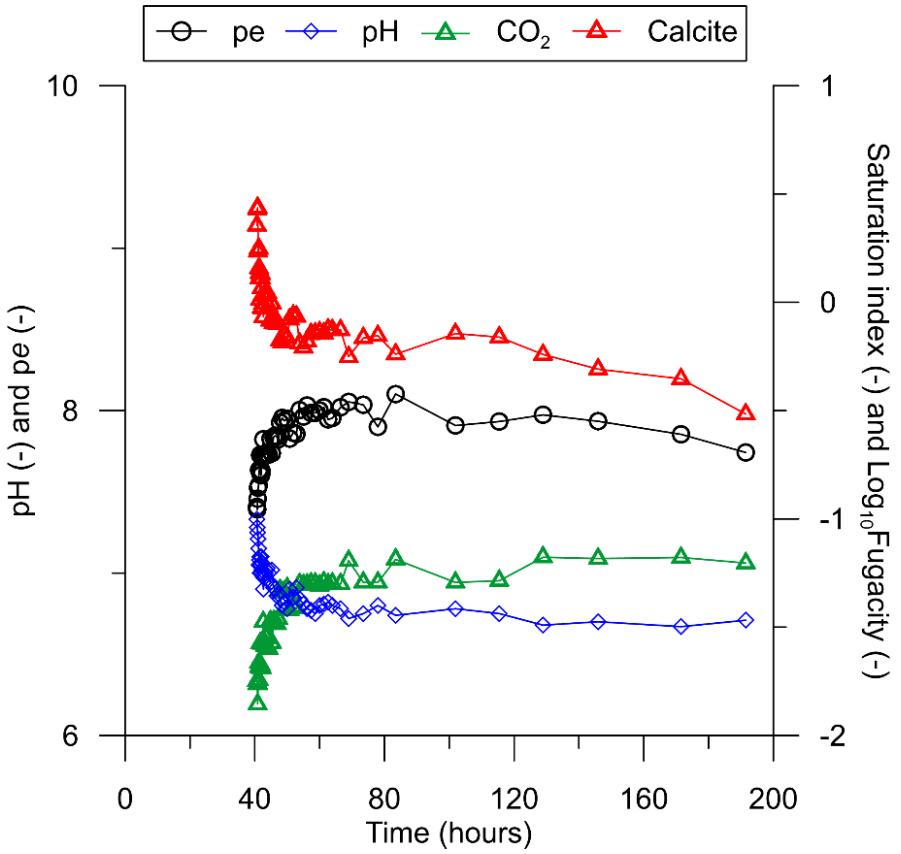


Figure 7. pH, p*e*, Calcite saturation index and $CO_2$ fugacity as calculated by PHREEQC-3 geochemical model.

459 The dolomite mimicked the behaviour of calcite (not shown). This highlights the presence of calcium
460 and magnesium salts that have been rapidly dissolved by the incoming rainwater, while more stable
461 carbonates, abundant in these soils (Tab. 1), are less prone to be readily dissolved. A clear inverse
462 relationship between $CO_2$ partial pressure and pH is also visible from Figure 8. This is due to the pH
463 decrease, which in turn drives the speciation of DIC in natural waters from $HCO_3^-$ dominated to $CO_2$
464 dominated (Parkhurst and Appelo 2013).
465 Finally, the $Cl^-$ cumulative mass flux is estimated to be 200.1 mmol/m$^2$, which is an elevated value
466 for a freshwater agricultural environment in a temperate climate. This aspect should be further studied
467 in relation with climate changes, since recently it has been shown that $Cl^-$ mass balance and heat flux
468 modelling provide insights on climate effects on aquifer recharge (Irvine et al. 2018).
469 The present results highlight the need to study in detail the impact that climate change can induce on
470 local and site-specific mechanisms such as the percolation of dissolved species towards groundwater
471 resources and the processes that regulate nitrogen cycle in agricultural soils. To do so, downscaling
472 of "Global Drivers" outcomes to the watershed scale is urgently needed. For the Po river basin, recent
473 literature has shown that temperature is expected to increase in the whole basin and in all the seasons
474 (Dell'Aquila et al. 2012; Vezzoli et al. 2015). The most significant changes in precipitations and
475 discharges are expected to occur in summer when the reduction of precipitation will lead to low flow
476 persistence; and in autumn-winter time where concentrated precipitation events will increase the high
477 flows frequency (Vezzoli et al. 2015). Thus, not only climate change will affect rainfalls and
478 discharge pattern in this watershed, but the increase of droughts periods followed by extreme
479 precipitations events will probably trigger increased solutes concentration in recharge water, together
480 with the so far unaccounted $NO_2^-$ leaching. The main limitation of the proposed approach is that only
481 a single extreme rainfall event was simulated, while the effect of different rainfall intensity should be
482 explored in the future. For example, Wu et al. (2018) have recently investigated the reactive N losses
483 in run-off waters with different rainfall intensities and terrain slopes, although they did not investigate
484 the fate of reactive N within the soil. In addition, future studies should also evaluate the use of

485 different soils or different fertilization timing and rates in combination with extreme rainfall events.
486 Besides, considering that extreme events will possibly trigger nitrite leaching and not only nitrate,
487 this could influence the existing management and protection plans of shallow aquifers that are mainly
488 focused on monitoring the latter contaminant (Haas et al. 2017). Moreover, the existing vulnerability
489 methods (Stigter et al., 2006; Busico et al., 2017), should be further modified to include partial
490 denitrification effects in presence of shallow aquifers. Finally, studies on $N_2O$ soils productions
491 (Giguere et al. 2017) and nitrous acid (Su et al. 2011) release in atmosphere should also take into
492 account the effects of extreme rainfall events.
493
494 **5. CONCLUSIONS**
495
496 This paper describes and quantifies the $NO_2^-$ leaching behaviour from agricultural soils depleted in
497 organic matter subjected to extreme rainfall events. The study was developed by means of soil
498 sampling in the field and unsaturated/saturated intact soil column experiment. Soil extraction showed
499 that accumulated $NO_2^-$ could be significantly leached by extreme rainfall events from these soils. The
500 soil column experiment highlighted elevated $NO_3^-$ and $NO_2^-$ concentrations in the leachate, and the
501 reactive flow and transport model well simulated the behaviour of the tracers and reactive species
502 allowing the quantification of cumulative mass fluxes. $NO_2^-$ production was mainly due to incomplete
503 denitrification and much less due to incomplete nitrification processes. The incomplete denitrification
504 was caused by lack of available labile organic substrates and not by other inhibitory effects, like for
505 example changes in pH.
506 This study, for the first time, put on evidence that the mechanism for $NO_2^-$ accumulation in soils is
507 related to the lack of available labile organic substrates, suggesting that leaching of $NO_2^-$ towards the
508 saturated zone in the event of extreme rainfalls could arise from agricultural soils depleted in labile
509 fraction of organic carbon due to incomplete denitrification. This process could be exacerbated in the
510 Mediterranean region, where climate changes already have created the conditions for the recurrence

511 of alternating of prolonged dry periods favouring salts accumulation and extreme rainfall events
512 favouring saturated water conditions and salts leaching. Finally, the results of the column experiment
513 highlight the relevance of closely spaced sampling intervals to "capture" the effect of extreme rainfall
514 events on the fate of reactive N in agricultural soils. Thus, new approaches to continuously monitor
515 pore-water and groundwater reactive N species are needed in field applications. The results found in
516 this study cannot be directly transferred to other soil types, but the approach here proposed could be
517 used to quantify if $NO_2^-$ accumulation and leaching could be relevant or not.
518
519 **Acknowledgements**
520
521 This work was financially supported by the Emilia-Romagna Region within the Rural Development
522 Programme (PSR) 2014-2020 and within the POR FESR 2007-2013 Programme for the development
523 of the regional High Technology Network. The authors would like to thank Dr. Erica Racchetti
524 (Department of Chemistry, Life Sciences and Environmental Sustainability, University of Parma) for
525 helping with chromatographic analyses. We would like to thank two anonymous reviewers for their
526 valuable comments and remarks that have helped to improve the clarity of this manuscript.
527
528 **References**
529
530 Allen, R.G., Pereira, L.S., Raes, D., Smith, M., 1998. Crop Evapotranspiration. Guidelines for
531 Computing Crop Water Requirements. FAO Irrigation and Drainage Paper 56 FAO, Rome.
532
533 Antolini, G., Auteri, L., Pavan, V., Tomei, F., Tomozeiu, R., Marletto, V., 2016. A daily high-
534 resolution gridded climatic data set for Emilia-Romagna, Italy, during 1961–2010. International
535 Journal of Climatology, 36(4), 1970-1986. DOI: 10.1002/joc.4473.
536

ASTM, 2010. Standard test method for density of soil in place by the drive-cylinder method. D2937–10.

Borken, W., Matzner, E., 2009. Reappraisal of drying and wetting effects on C and N mineralization and fluxes in soils. Global Change Biology, 15(4), 808-824. DOI: 10.1111/j.1365-2486.2008.01681.x.

Busico, G., Kazakis, N., Colombani, N., Mastrocicco, M., Voudouris, K., Tedesco, D., 2017. A modified SINTACS method for groundwater vulnerability and pollution risk assessment in highly anthropized regions based on $NO_3^-$ and $SO_4^{2-}$ concentrations. Science of the Total Environment, 609, 1512-1523. DOI: 10.1016/j.scitotenv.2017.07.257.

Castaldelli, G., Colombani, N., Soana, E., Vincenzi, F., Fano, E.A., Mastrocicco, M. 2019. Reactive nitrogen losses via denitrification assessed in saturated agricultural soils. Geoderma, 337, 91-98. DOI: 10.1016/j.geoderma.2018.09.018.

Castaldelli, G., Colombani, N., Tamburini, E., Vincenzi, F., Mastrocicco, M., 2018. Soil type and microclimatic conditions as drivers of urea transformation kinetics in maize plots. Catena, 166, 200-208. DOI: 10.1016/j.catena.2018.04.009

Castaldelli, G., Colombani, N., Vincenzi, F., Mastrocicco, M., 2013a. Linking dissolved organic carbon, acetate and denitrification in agricultural soils. Environmental Earth Sciences, 68(4), 939-945. DOI: 10.1007/s12665-012-1796-7.

Castaldelli, G., Soana, E., Racchetti, E., Pierobon, E., Mastrocicco, M., Tesini, E.A., Fano, E., Bartoli, M., 2013b. Nitrogen budget in a lowland coastal area within the Po river basin (Northern Italy):

563 multiple evidences of equilibrium between sources and internal sinks. Environmental Management,
564 52(3), 567-580. DOI: 10.1007/s00267-013-0052-6.
565
566 Chen, Z., Ding, W., Xu, Y., Müller, C., Rütting, T., Yu, H., JFan, J., Zhang, J., Zhu, T., 2015.
567 Importance of heterotrophic nitrification and dissimilatory nitrate reduction to ammonium in a
568 cropland soil: evidences from a $^{15}N$ tracing study to literature synthesis. Soil Biology and
569 Biochemistry, 91, 65-75. DOI: 10.1016/j.soilbio.2015.08.026.
570
571 Colombani, N., Di Giuseppe, D., Faccini, B., Mastrocicco, M., Coltorti, M., 2016. Formation and
572 dissolution of salt crusts as a rapid way of nitrate mobilization in a tile-drained agricultural field under
573 a temperate climate. Arabian Journal of Geosciences, 9(6), 463. DOI: 10.1007/s12517-016-2473-z.
574
575 Colombani, N., Mastrocicco, M., Di Giuseppe, D., Faccini, B., Coltorti, M., 2014. Variation of the
576 hydraulic properties and solute transport mechanisms in a silty-clay soil amended with natural
577 zeolites. Catena, 123, 195-204. DOI: 10.1016/j.catena.2014.08.003.
578
579 Costa, J.L., Massone, H., Martınez, D., Suero, E.E., Vidal, C.M., Bedmar, F., 2002. Nitrate
580 contamination of a rural aquifer and accumulation in the unsaturated zone. Agricultural Water
581 Management, 57(1), 33-47. DOI: 10.1016/S0378-3774(02)00036-7.
582
583 Dell'Aquila, A., Calmanti, S., Ruti, P., Struglia, M.V., Pisacane, G., Carillo, A., Sannino, G., 2012.
584 Effects of seasonal cycle fluctuations in an A1B scenario over the Euro-Mediterranean region.
585 Climate Research, 52, 135-157. DOI: 10.3354/cr01037.
586

587 Di, H.J., Cameron, K.C., 2002. Nitrate leaching in temperate agroecosystems: sources, factors and
588 mitigating strategies. Nutrient Cycling in Agroecosystems, 64(3), 237-256. DOI:
589 10.1023/A:1021471531188.
590
591 Durner, W. 1994. Hydraulic conductivity estimation for soils with heterogeneous pore structure.
592 Water Resources Research, 30(2),211-223. DOI: 10.1029/93WR02676
593
594 Erisman, J. W., Sutton, M. A., Galloway, J., Klimont, Z., Winiwarter, W. 2008. How a century of
595 ammonia synthesis changed the world. Nature Geoscience, 1(10), 636. DOI: 10.1038/ngeo325.
596
597 Erskine, A.D., 2000. Transport of ammonium in aquifers: retardation and degradation. Quarterly
598 Journal of Engineering Geology and Hydrogeology, 33 (2), 161-170. DOI: 10.1144/qjegh.33.2.161.
599
600 Friedl, J., De Rosa, D., Rowlings, D.W., Grace, P.R., Müller, C., Scheer, C., 2018. Dissimilatory
601 nitrate reduction to ammonium (DNRA), not denitrification dominates nitrate reduction in subtropical
602 pasture soils upon rewetting. Soil Biology and Biochemistry, 125, 340-349. DOI:
603 10.1016/j.soilbio.2018.07.024.
604
605 Gelfand, I., Yakir, D., 2008. Influence of nitrite accumulation in association with seasonal patterns
606 and mineralization of soil nitrogen in a semi-arid pine forest. Soil Biology and Biochemistry, 40(2),
607 415-424. DOI: 10.1016/j.soilbio.2007.09.005.
608
609 Giguere, A.T., Taylor, A.E., Suwa, Y., Myrold, D.D., Bottomley, P.J., 2017. Uncoupling of ammonia
610 oxidation from nitrite oxidation: impact upon nitrous oxide production in non-cropped Oregon soils.
611 Soil Biology and Biochemistry, 104, 30-38. DOI: 10.1016/j.soilbio.2016.10.011.
612

613 Haas, M.B., Guse, B., Fohrer, N., 2017. Assessing the impacts of Best Management Practices on
614 nitrate pollution in an agricultural dominated lowland catchment considering environmental
615 protection versus economic development. Journal of Environmental Management, 196, 347-364.
616 DOI: 10.1016/j.jenvman.2017.02.060.
617
618 Hill, M.C., 2006. The practical use of simplicity in developing ground water models. Groundwater,
619 44(6), 775-781. DOI: 10.1111/j.1745-6584.2006.00227.x.
620
621 Hillel, D., 1998. Environmental soil physics: Fundamentals, applications, and environmental
622 considerations. Elsevier.
623
624 Irvine, D.J., Kurylyk, B.L., Cartwright, I., Bonham, M., Post, V.E., Banks, E.W., Simmons, C.T.,
625 2017. Groundwater flow estimation using temperature-depth profiles in a complex environment and
626 a changing climate. Science of The Total Environment, 574, 272-281.
627
628 Köhne, J.M., Köhne, S., Šimůnek, J., 2009. A review of model applications for structured soils: a)
629 Water flow and tracer transport. Journal of Contaminant Hydrology, 104(1-4), 4-35. DOI:
630 10.1016/j.jconhyd.2008.10.002.
631
632 Kramer, S. B., Reganold, J.P., Glover, J.D., Bohannan, B.J., Mooney, H.A. 2006. Reduced nitrate
633 leaching and enhanced denitrifier activity and efficiency in organically fertilized soils. Proceedings
634 of the National Academy of Sciences, 103(12), 4522-4527. DOI: 10.1073/pnas.0600359103
635
636 Jiao, Y., Hendershot, W.H., Whalen, J.K., 2004. Agricultural practices influence dissolved nutrients
637 leaching through intact soil cores. Soil Science Society of America Journal, 68(6), 2058-2068. DOI:
638 10.2136/sssaj2004.2058.

639

640 Larsson, M.H., Jarvis, N.J., 1999. Evaluation of a dual-porosity model to predict field-scale solute
641 transport in a macroporous soil. Journal of Hydrology, 215(1-4), 153-171. DOI: 10.1016/S0022-
642 1694(98)00267-4.

643

644 Lee, J., Horton, R., Jaynes, D.B., 2002. The feasibility of shallow time domain reflectometry probes
645 to describe solute transport through undisturbed soil columns. Soil Science Society of America
646 Journal, 66, 53-57. DOI: 10.2136/sssaj2002.5300.

647

648 Lim, N.Y., Frostegård, Å., Bakken, L.R., 2018. Nitrite kinetics during anoxia: The role of abiotic
649 reactions versus microbial reduction. Soil Biology and Biochemistry, 119, 203-209. DOI:
650 10.1016/j.soilbio.2018.01.006.

651

652 Ma, L., Shan, J., Yan, X., 2015. Nitrite behaviour accounts for the nitrous oxide peaks following
653 fertilization in a fluvo-aquic soil. Biology and fertility of soils, 51(5), 563-572. DOI: 10.1007/s00374-
654 015-1001-8.

655

656 Maggi, F., Daly, E., 2013. Decomposition pathways and rates of human urine in soils. Journal of
657 Agricultural and Food Chemistry, 61(26), 6175-6186. DOI: 10.1021/jf401212n

658

659 Maharjan, B., Venterea, R.T., 2013. Nitrite intensity explains N management effects on $N_2O$
660 emissions in maize. Soil Biology and Biochemistry, 66, 229-238. DOI:
661 10.1016/j.soilbio.2013.07.015.

662

663 Mastrocicco, M., Colombani, N., Castaldelli, G., 2019. Direct measurement of dissolved dinitrogen
664 to refine reactive modelling of denitrification in agricultural soils. Science of The Total Environment,
665 647, 134-140. DOI: 10.1016/j.scitotenv.2018.07.428.
666
667 Mastrocicco, M., Colombani, N., Salemi, E., Castaldelli, G., 2011. Reactive modeling of
668 denitrification in soils with natural and depleted organic matter. Water, Air and Soil Pollution, 222(1-
669 4), 205-215. DOI: 10.1007/s11270-011-0817-6.
670
671 Nash, J.E., Sutcliffe, J.V., 1970. River flow forecasting through conceptual models part I - A
672 discussion of principles. Journal of Hydrology 10(3), 282-290. DOI: 10.1016/0022-1694(70)90255-
673 6.
674
675 Nkoa, R. 2014. Agricultural benefits and environmental risks of soil fertilization with anaerobic
676 digestates: a review. Agronomy for Sustainable Development, 34(2), 473-492. DOI:
677 doi.org/10.1007/s13593-013-0196-z.
678
679 Oh, J., Silverstein, J., 1999. Acetate limitation and nitrite accumulation during denitrification. Journal
680 of Environmental Engineering, 125(3), 234-242. DOI: 10.1061/(ASCE)0733-9372(1999)125:3(234).
681
682 Parkhurst DL, Appelo CAJ, 2013. Description of input and examples for PHREEQC version 3. A
683 computer program for speciation, batch-reaction, one-dimensional transport, and inverse geochemical
684 calculations: U.S. Geological Survey Techniques and Methods. Book 6, Chap. A43, p 497. Available
685 only at https://pubs.usgs.gov/tm/06/a43.
686

687 Perfect, E.M.C.S., Sukop, M.C., Haszler, G.R., 2002. Prediction of dispersivity for undisturbed soil
688 columns from water retention parameters. Soil Science Society of America Journal, 66(3), 696-701.
689 DOI:10.2136/sssaj2002.6960.
690
691 Philips, S., Laanbroek, H.J., Verstraete, W., 2002. Origin, causes and effects of increased nitrite
692 concentrations in aquatic Environments. Reviews in Environmental Science and Bio/Technology, 1,
693 115. DOI: 10.1023/A:1020892826575.
694
695 Riley, W. J., Ortiz-Monasterio, I., Matson, P. A., 2001. Nitrogen leaching and soil nitrate, nitrite, and
696 ammonium levels under irrigated wheat in Northern Mexico. Nutrient Cycling in Agroecosystems,
697 61(3), 223-236. DOI: 10.1023/A:1013758116346.
698
699 Rivett, M.O., Buss, S.R., Morgan, P., Smith, J.W., Bemment, C.D., 2008. Nitrate attenuation in
700 groundwater: a review of biogeochemical controlling processes. Water Research, 42(16), 4215-4232.
701 DOI: 10.1016/j.watres.2008.07.020.
702
703 Shen, Q.R., Ran, W., Cao, Z.H., 2003. Mechanisms of nitrite accumulation occurring in soil
704 nitrification. Chemosphere, 50(6), 747-753. DOI: 10.1016/S0045-6535(02)00215-1.
705
706 Šimůnek, J., Šejna, M., Saito, H., Sakai, M., van Genuchten, M.T., 2009. The HYDRUS-1D Software
707 Package for Simulating the Movement of Water, Heat, and Multiple Solutes in Variably Saturated
708 Media, Version 4.08, HYDRUS Software Series 3, Department of Environmental Sciences,
709 University of California Riverside, Riverside, California, USA; 315.
710
711 Stigter, T.Y., Ribeiro, L., Dill, A.C., 2006. Evaluation of an intrinsic and a specific vulnerability
712 assessment method in comparison with groundwater salinisation and nitrate contamination levels in

713 two agricultural regions in the south of Portugal. Hydrogeology Journal, 14(1-2), 79-99. DOI:
714 doi.org/10.1007/s10040-004-0396-3.
715
716 Su, H., Cheng, Y., Oswald, R., Behrendt, T., Trebs, I., Meixner, F.X., Andreae, M.O., Cheng, P.,
717 Zhang, Y., Pöschl, U. (2011). Soil nitrite as a source of atmospheric HONO and OH radicals. Science,
718 1207687. DOI: 10.1126/science.1207687.
719
720 Taylor, P.G., Townsend, A.R., 2010. Stoichiometric control of organic carbon–nitrate relationships
721 from soils to the sea. Nature, 464, 1178-1181. DOI: 10.1038/nature08985.
722
723 Tierling, J., Kuhlmann, H., 2018. Emissions of nitrous oxide ($N_2O$) affected by pH-related nitrite
724 accumulation during nitrification of N fertilizers. Geoderma, 310, 12-21. DOI:
725 10.1016/j.geoderma.2017.08.040.
726
727 Tilman, D., Fargione, J., Wolff, B., D'antonio, C., Dobson, A., Howarth, R., Schindler, D.,
728 Schlesinger, W.H., Simberloff, D., Swackhamer, D., 2001. Forecasting agriculturally driven global
729 environmental change. Science, 292(5515), 281-284. DOI: 10.1126/science.1057544.
730
731 Van Cleemput, O., Samater, A.H., 1995. Nitrite in soils: accumulation and role in the formation of
732 gaseous N compounds. Fertilizer Research, 45(1), 81-89. DOI: doi.org/10.1007/BF00749884.
733
734 van Genuchten, M.T., 1980. A closed-form equation for predicting the hydraulic conductivity of
735 unsaturated soils. Soil Science Society of America Journal, 44(5), 892-898. DOI:
736 10.2136/sssaj1980.03615995004400050002x.
737

738 van Genuchten, M.T., 1985. Convective-dispersive transport of solutes involved in sequential first-
739 order decay reactions. Computers & Geosciences, 11(2), 129-147. DOI: 10.1016/0098-
740 3004(85)90003-2.
741
742 van Grinsven, H. J., Bouwman, L., Cassman, K. G., van Es, H. M., McCrackin, M. L., Beusen, A. H.
743 2015. Losses of ammonia and nitrate from agriculture and their effect on nitrogen recovery in the
744 European Union and the United States between 1900 and 2050. Journal of Environmental Quality,
745 44(2), 356-367. DOI: 10.2134/jeq2014.03.0102.
746
747 Venterea, R.T., Clough, T.J., Coulter, J.A., Breuillin-Sessoms, F., Wang, P., Sadowsky, M.J., 2015.
748 Ammonium sorption and ammonia inhibition of nitrite-oxidizing bacteria explain contrasting soil
749 $N_2O$ production. Scientific Reports, 5, 12153. DOI: 10.1038/srep12153.
750
751 Ventura, M., Scandellari, F., Ventura, F., Guzzon, B., Rossi Pisa, P., Tagliavini, M., 2008. Nitrogen
752 balance and losses through drainage waters in an agricultural watershed of the Po Valley (Italy).
753 European Journal of Agronomy 29, 108-115. DOI: 10.1016/j.eja.2008.05.002.
754
755 Vezzoli, R., Mercogliano, P., Pecora, S., Zollo, A.L., Cacciamani, C., 2015. Hydrological simulation
756 of Po River (North Italy) discharge under climate change scenarios using the RCM COSMO-CLM.
757 Science of the Total Environment, 521, 346-358. DOI: 10.1016/j.scitotenv.2015.03.096.
758
759 Vogeler, I., Clothier, B.E., Green, S.R., Scotter, D.R., Tillman, R.W., 1996. Characterizing water and
760 solute movement by time domain reflectometry and disk permeametry. Soil Science Society of
761 America Journal, 60(19), 5-12. DOI: 10.2136/sssaj1996.03615995006000010004x.
762

763 Wu, L., Peng, M., Qiao, S., Ma, X., 2018. Assessing impacts of rainfall intensity and slope on
764 dissolved and adsorbed nitrogen loss under bare loessial soil by simulated rainfalls. Catena, 170, 51-
765 63. Doi: 10.1016/j.catena.2018.06.007.
766
767 Zhang, D., Beven, K., Mermoud, A., 2006. A comparison of non-linear least square and GLUE for
768 model calibration and uncertainty estimation for pesticide transport in soils. Advances in Water
769 Resources, 29(12), 1924-1933. DOI: 10.1016/j.advwatres.2006.02.004.